

COVER PAGE

Document downloaded by @DAEL

Thu Nov 26 20:15:11 2026
For personal use

When automatic English translation is provided, only the original document is authentic.
The EAA cannot be held responsible of any translation error

Bibliographical reference

Noise Reduction of Circular and Non-Circular Jets Surrounded by Annular Swirl Flow, P. Balakrishnan and K. Srinivasan, Acta Acustica **vol. 103** (Number 5), 2017, pp. 732-745

DOI
https://doi.org/10.3813/AAA.919102

Acta Acustica united with Acustica
Vol. 103 (2017) 732 – 745

DOI 10.3813/AAA.919102

Noise Reduction of Circular and Non-Circular Jets Surrounded by Annular Swirl Flow

P. Balakrishnan, K. Srinivasan
Department of Mechanical Engineering IIT Madras, Chennai – 600036, India. ksri@iitm.ac.in

Summary
An experimental study of the acoustic far field and flow field of co-axial circular and non-circular jets with the vane angles of 0° and 30° are presented in this paper. Flat vanes are fixed in the annular passage of the co-axial jets, which cause trailing edge vortices and/or swirl flow. The co-axial jets with vane angles of 0° and 30° almost eliminate the transonic tones and screech tones entirely, in contrast to non-swirl jet. The broadband shock associated noise is also mitigated by the co-axial jets, irrespective of the vane angles. The co-axial jets are efficient in overall noise suppression at both subsonic and supersonic conditions. The co-axial jets diminish the low frequency noise and enhance the high frequency noise. Reduction in core length is highest for the co-axial jets compared to the non-swirl jet. The flow visualization study also confirms that the co-axial jets weaken or destroy the shock cells and reduce the number of the shock cells compared to non-swirl jet.

PACS no. 43.28.Ra, 43.50.Nm

1. Introduction

Jet noise reduction has important implications in both human and material considerations. The noise radiated from high speed jets majorly comprise mixing noise, shock associated noise and screech tones. Reduction and mitigation of noise at supersonic conditions is a major engineering challenge in aerospace applications. In addition to human ailments, noise can cause material failure of nearby structures by acoustic fatigue.

The present work aims to augment jets of various cross-sections with passive co-axial swirlers and study the effect on the noise emitted. Experiments are carried out on circular and non-circular (ellipse and square) primary jets surrounded by co-axial swirling flow in the annular passage. The results are compared with a non-swirl or free jet for same operating conditions. In order to further delineate the effect of swirl, two vane angles (0° and 30°) of the co-axial swirler are considered. Although the 0° vanes do not induce a tangential velocity, the vortices shed from the downstream of the vanes cause turbulent interactions with the primary jet fluid and can diminish the core length compared to the non-swirl jet. Co-axial swirlers with 30° vanes impose a tangential velocity. However, the non-swirl jet or free jet does not produce considerable vortices or tangential velocity compared with co-axial jets with the vanes installed in the annular region.

Received 5 May 2016,
accepted 2 July 2017.

1.1. Flow structures of free, non-circular and co-axial swirl jet

The free jet usually consists of a potential core region in subsonic conditions or shock-dominated region under imperfectly expanded conditions. It is followed by a transition region and finally, a self-similar region. The velocity is constant throughout in the potential core region, which extends up to 4 to 6D. In the transition region, the centerline velocity begins to decrease and this region extends up to 6 to 20D. However for supersonic conditions a shock cell system commences from the exit of the nozzle due to the mismatch of the pressure between the jet and the ambient fluid. The strength and extent of the shock cell region depends on the nozzle exit diameter (D) and NPR. The flow structure of an under expanded supersonic non-swirl jet is shown in Figure 1.

Non-circular free jets such as elliptical, square and triangular jets have been studied by several researchers [1, 2, 3]. It is well known that the non-circular jets enhance the jet spread, velocity decay and promote turbulent mixing compared to circular jets.

Swirl is another flow control tool that has been effectively used for mixing applications. The effects of the addition of swirl to an axial stream have been extensively discussed [4, 5, 6]. Like non-circular jets, swirl also enhances the entrainment rates and increases the turbulence levels and mixing. This study is a unique attempt to combine two successful passive strategies (swirl and non-circularity) for noise reduction potential.

The schematic of a co-axial swirl jet is shown in Figure 2. The flow structures in a co-axial swirl jet are different from that of a non-swirl jet. It consists of primary

© S. Hirzel Verlag · EAA

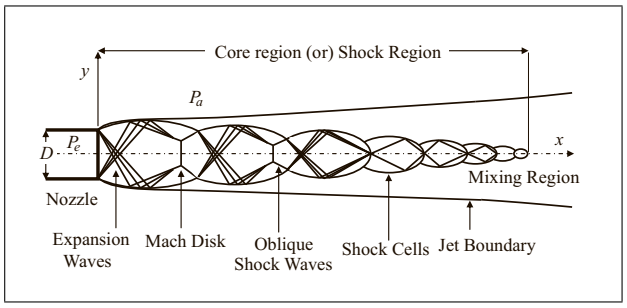

Figure 1. Flow structure of an under expanded non-swirl jet.

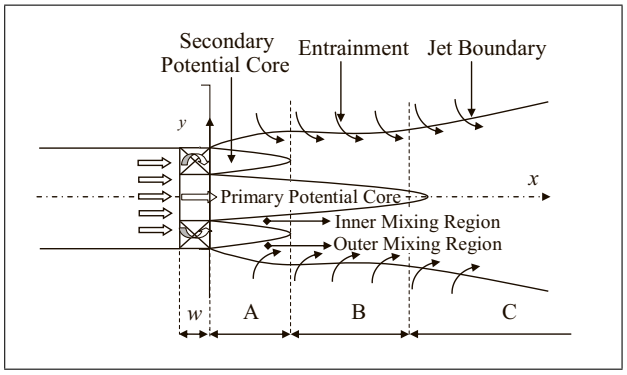

Figure 2. Flow structures of co-axial swirl jet. *w*: Width of the Swirler, A: Initial merging region, B: Intermediate region, C: Fully merged region.

and secondary potential cores and primary and secondary shear layers. The primary core decay largely depends on the vane angles in the annular passage in both subsonic and supersonic conditions. The secondary core usually disappears in the initial merging zone and the both primary and secondary core shear layer merge in the intermediate regions. However, for supersonic conditions the shocks may exist in both primary and secondary cores and may interact with each other depending on the vane angle.

1.2. Acoustic characteristics

The noise is generated from the interactions and mixing between the jet fluid and ambient fluid. The noise types can be transonic tones, screech tones, turbulent mixing noise and broadband shock associated noise. The transonic tones are generated due to the unsteadiness of shock oscillations at low NPRs [7]. The screech tones are generated due to the feedback loop, which triggers the new instability waves from the exit of nozzles. The mixing between the jet fluid and ambient generates turbulent mixing noise. Shock associated noise originates from the interactions of shock cells with the large scale structures convecting downstream. Furthermore, when the large scale structures are convected downstream at supersonic speeds relative to ambient conditions, Mach waves are generated [8]. These are the dominant noise sources at high speed conditions for a non-swirl or free jet.

Lu *et al.* [9] conducted experimental work on the acoustic effect of vanes installed at circumferential locations of

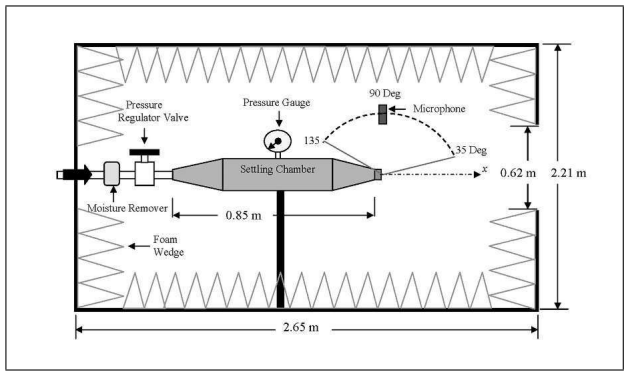

Figure 3. Layout of anechoic chamber.

an engine model. It was observed that at low pressure ratios (1.1 to 1.5), the swirl jet noise is broadband and similar to non-swirl jet noise. Further, they observed that the swirl jet noise is higher than non-swirl jet at upstream angles and therefore, noise attenuation is possible only at downstream angles. The tangential injection swirl generation study by Yu and Chen [10] for supersonic conditions observed that the screech tones are present in both non-swirl and swirl jets. The effect of tabs on the flow field and noise was studied by Samimy *et al.* [11], who concluded that the tabs weaken the shock cells compared to no tab cases. Papamoschou and Marco [12] used co-flow to reduce the far field noise of a free jet by 5 dB at a Mach number of 1.5. Kiran [13] studied a subsonic co-flowing nozzle with chevron lips and found that the dominant noise sources were located at the end of the potential core. Further, he added that the chevron nozzle reduced the low frequency noise compared to the base line jet.

2. Experimental methods and procedures

2.1. Anechoic chamber and instrumentation

The experiments are carried out in the anechoic chamber installed at the Thermodynamics and Combustion Engineering Laboratory, Department of Mechanical Engineering, IIT Madras. The ambient air is compressed using a Khosla compressor (150 HP) located outside the laboratory. The pressure in the settling chamber is continuously monitored from a Bourdon type pressure gauge and a piezo-resistive pressure transducer. The layout of anechoic chamber is shown in Figure 3, and the lower cut-off frequency of the chamber is 700 Hz.

Only cold jets have been investigated in the present study. The acoustic far field measurements are carried out using a ¼-inch condenser microphone (PCB 377A01) with a sensitivity of 4 mV/Pa. The centerline pressure measurements are carried out using a pitot probe connected to a piezo-resistive pressure transducer (Endevco Model 8510C-100) and to the data acquisition system. The acoustic and flow field data are acquired at a sampling rate of 150,000 samples/sec. A high speed digital camera (Mikrotron MC1302) is used for the flow visualization study. For acquiring the data, a National Instruments data

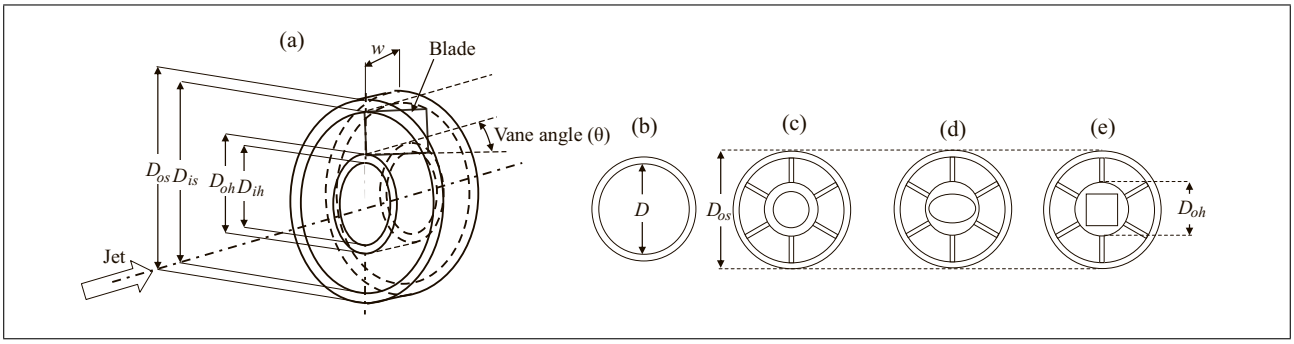

Figure 4. Co-axial jet configurations. (a) Co-axial swirler with dimensions (only one blade shown here), (b) Non-swirl jet, (c) Co-axial circular jet, (d) Co-axial ellipse jet, (e) Co-axial square jet.

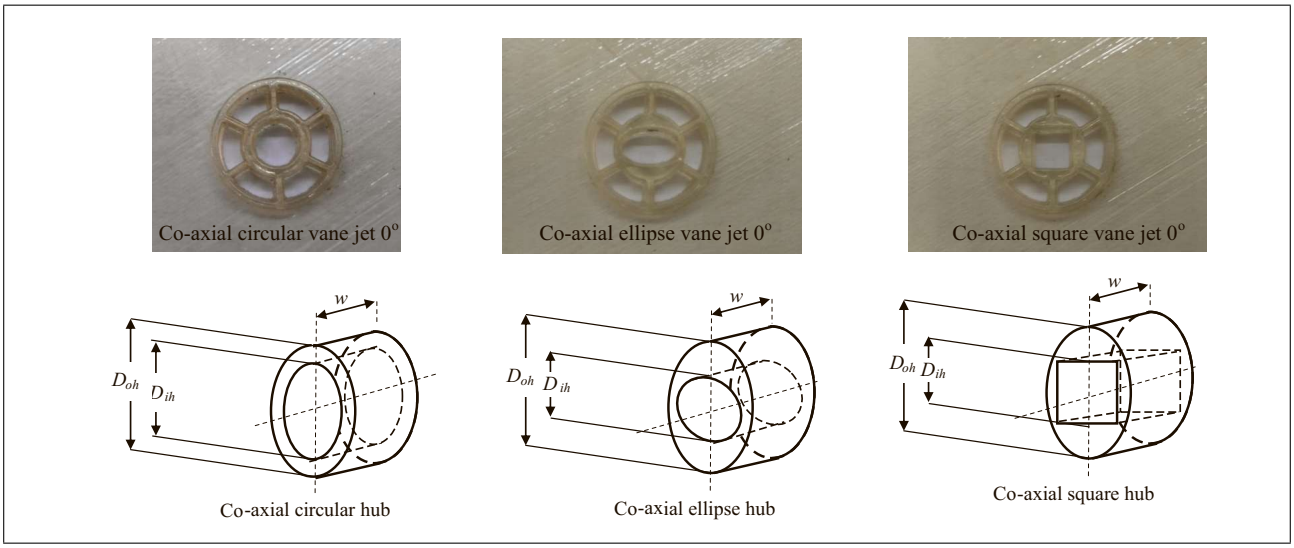

Figure 5. Photographs of the co-axial jet models and schematic of the central hubs. Top row: Photographs of the co-axial vane jets at the vane angle of 0°. Bottom row: Center hubs of the co-axial vane jets (Hubs only shown here without annular vanes).

acquisition board NI-PCI-6143 is used, which is controlled by Labview 14.

2.2. Test models and methods of measurements

The schematic of co-axial swirl jet models (circular and non-circular) are shown in Figure 4.

The vanes are flat and fixed in the annular passage of the swirler at the required angle with respect to the jet axis, and the hub is allowed as a free jet or a single jet without any restrictions to the flow (refer Figure 5, bottom). Flat vane angles of 0° and 30° are considered in the present work. Flat vane angle of 30° produces swirl and the 0° vane generates vortices from the trailing edge of the vanes.

The dimensions of the annular passage are the same for both co-axial circular and co-axial non-circular jets. The term 'co-axial circular jet' means that the central hub houses a circular shaped jet that is surrounded by annular vanes (Figure 4c). Similarly, 'co-axial non- circular jet' means that the central hub has non-circular cut-outs that are ellipse or square shaped with annular vanes (Figures 4d and 4e). All the central hubs of the co-axial circular and co-axial non-circular jet devices have equal areas and are extruded straight. Figure 5 shows the photographs of the co-axial jet models and the schematics of the hubs showing the extrusion.

The swirl jet outer (D_{os}) and internal (D_{is}) diameters are 16 and 14 mm, respectively. Similarly, the hub internal (D_{ih}) and external (D_{oh}) diameters are 9 and 6 mm, respectively. The blade thickness (t_b) is 1 mm and the number of blades (n) is 6. The width (w) of the jet model is 6 mm. The non-swirl jet is made with an outer diameter (D) of 12 mm to maintain the same equivalent area. The swirl jets are manufactured using Eden 350V Rapid Prototyping Machine at the Department of Engineering Design, IIT Madras and the material is photopolymer resin.

The acoustic far field measurements are carried out at $34D$ and the microphone measurements ranged from an upstream angle of 130° to a downstream angle of 35°. The nozzle pressure ratios (NPRs) ranged from 1.8 to 6.

3. Spectra of non-swirl and co-axial swirl jets

The acoustic spectra for the non-swirl and co-axial jets (circular, elliptical and square) with 0° and 30° vane angles are discussed in this section.

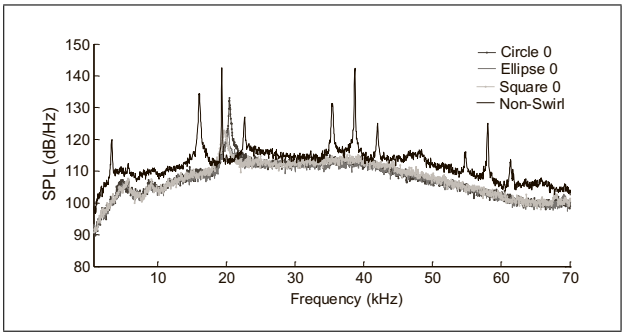

Figure 6. Far field sound pressure level spectra for NPR 1.8 and emission angle 90°.

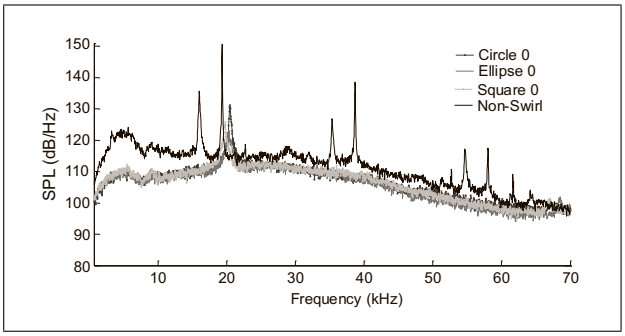

Figure 7. Far field sound pressure level spectra for NPR 1.8 and emission angle 35°.

3.1. Spectra of co-axial jets for 0° vane angle

Figure 6 and 7 shows the spectra for NPR 1.8 at an emission angle of 90° and 35°. Multiple transonic tones are observed for the non-swirl jet which is the noisiest at all the frequencies. However, the co-axial jet with 0° vane angle almost eliminates the transonic tones, except one peak at around 2 kHz. The noise radiated by the 0° vane angle jets are lower compared to the non-circular jet at all the frequencies. As mentioned earlier, the 0° vane angle jets induce trailing edge vortices from the vanes that enhances the mixing, resulting in lower noise levels compared to the non-swirl jet. At an emission angle of 35°, the amplitude of the transonic tone is higher compared to that at an emission angle of 90°. In addition, the low frequency noise level is also higher for all the jets at downstream angles due to the convection of the large scale turbulence structures in the downstream direction.

The transonic tones vanish at NPR 2 for all jets as shown in Figure 8 at an emission angle of 90°. However, the noise emerging from the 0° vane angle jets are higher compared to the non-swirl jet for frequencies more than 2.5 kHz. This is due to the breakup of fluid elements in the annular passages by the blades, leading to small scale turbulent structures which radiate high frequency noise.

Spectra at an upstream emission angle of 130° are shown in Figure 9, for NPR 4. A screech tone at a frequency of around 11.5 kHz and a BSAN hump are observed for the non-swirl jet. Similar results are observed for an emission angle of 90° at NPR 4, as shown in Figure 10. Yu and Chen [10] used tangential injection method

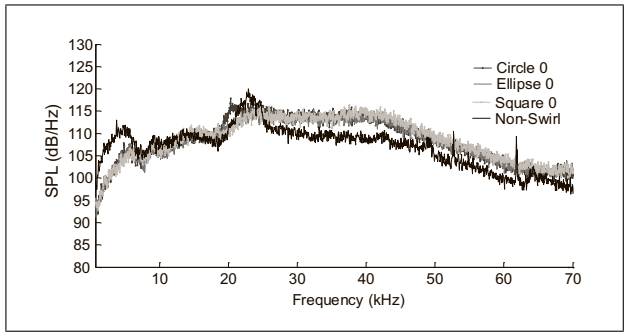

Figure 8. Far field sound pressure level spectra for NPR 2 and emission angle 90°.

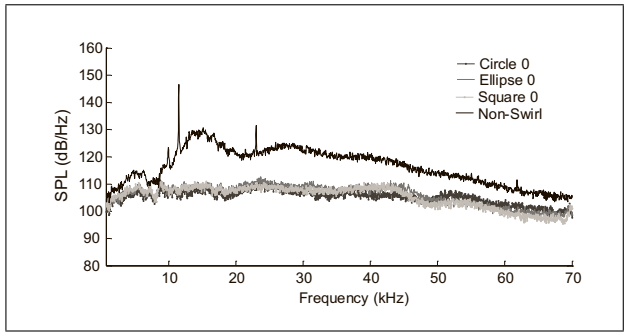

Figure 9. Far field sound pressure level spectra for NPR 4 and emission angle 130°.

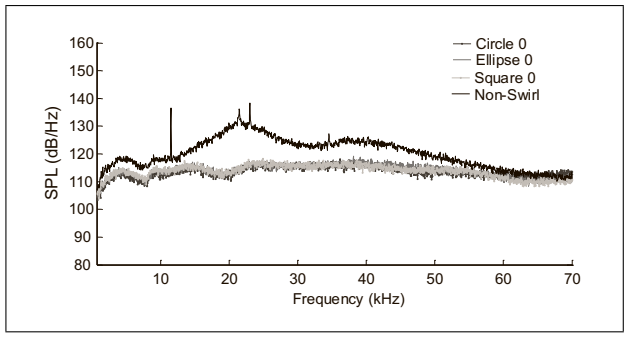

Figure 10. Far field sound pressure level spectra for NPR 4 and emission angle 90°.

for swirl generation and concluded that screech could not be eliminated by using swirl. However, the present co-axial flat vane method entirely eliminates the screech tone. It shows that the methods of generation of swirl plays an important role in eliminating the screech and BSAN. The strong shock cells and their interactions with the large scale structures causes screech tones and BSAN. However, the co-axial jets with 0° vane angle entirely eliminate the BSAN and screech tones. The enhanced entrainment rates and consequent weakening of the shock cells are the reasons for the interruption of the feedback loop and elimination of screech tones. In addition, the BSAN hump is widened for the emission angle of 90° compared to the emission angle of 35° for the non-swirl jet.

Spectra at the downstream angle of 35°, for NPR 4 are shown in Figure 11. BSAN is not observed for the emis-

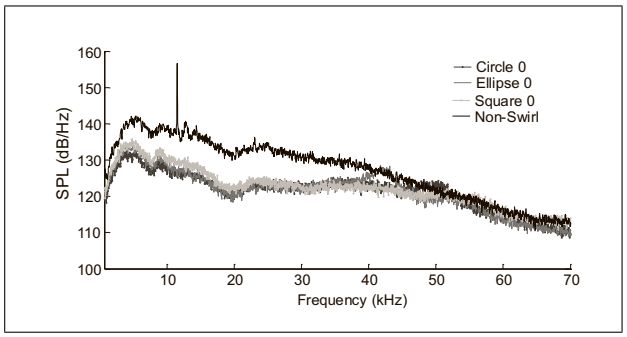

Figure 11. Far field sound pressure level spectra for NPR 4 and emission angle 35°.

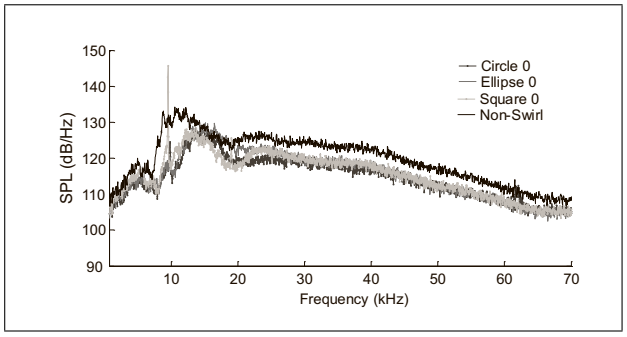

Figure 12. Far field sound pressure level spectra for NPR 6 and emission angle 130°.

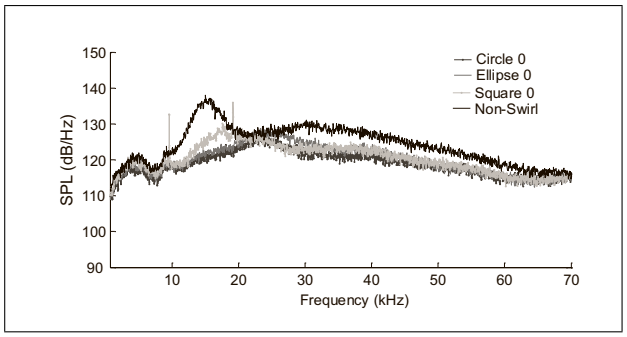

Figure 13. Far field sound pressure level spectra for NPR 6 and emission angle 90°.

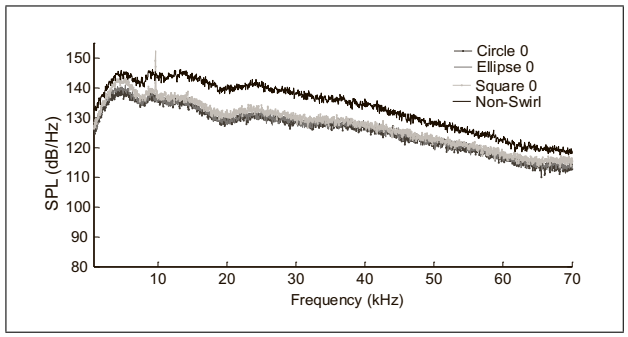

Figure 14. Far field sound pressure level spectra for NPR 6 and emission angle 35°.

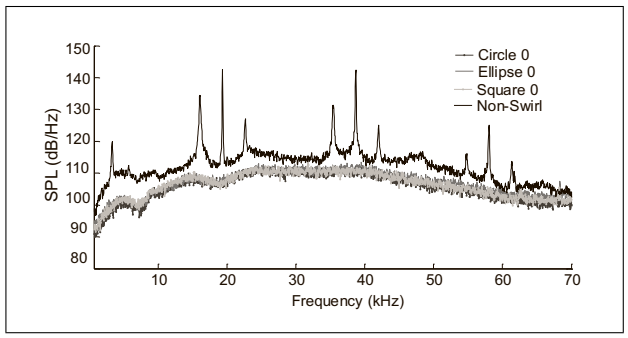

Figure 15. Far field sound pressure level spectra for NPR 1.8 and emission angle 90°.

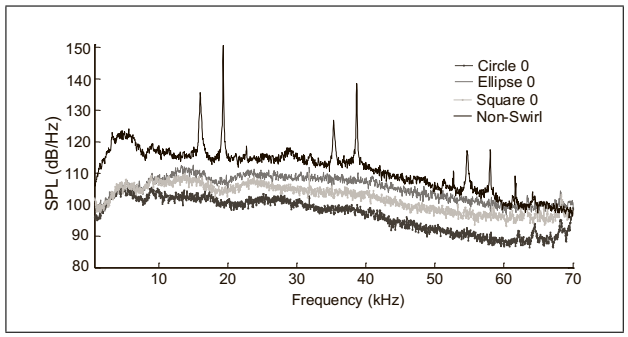

Figure 16. Far field sound pressure level spectra for NPR 1.8 and emission angle 35°.

sion angles lower than 65°, for the non-swirl jet. BSAN hump is observed for the non-swirl jet between the emission angle (EA), 130° > EA > 65° in the spectra. However, the screech tone exists for all the emission angles at NPR 4.

Strong BSAN levels are observed for the non-swirl jet at NPR 6, compared to NPR 4 for the emission angles of 130° and 90° as shown in Figures 12 and 13. Similarly, the co-axial jets with 0° vane angle also show weak BSAN peaks, and the co-axial square jet with 0° vane angle also shows screech tones. The increase in NPR causes strong shock cells, which are not completely eliminated by the 0° vane angle co-axial jets. Nevertheless, the co-axial jets with 0° vane angle are quieter than the non-swirl jet. At an emission angle of 35° for NPR 6, the spectra are shown in Figure 14. Screech tone still exists for the co-axial square jet with 0° vane angle, however the BSAN disappears for all the jets. From the spectral characteristics, it is clear that the screech tone exists for all the emission angles; however the BSAN gradually disappears as the observer moves towards downstream angles.

3.2. Spectra of co-axial jets for 30° vane angle

For the vane angle of 30°, there are no transonic tones emitted by the swirl jets (Figures 15 and 16), in contrast with jets from 0° vane angle jets where transonic tones are observed. The increase in vane angle leads to an increase the mixing and enhances the spread rates, thus resulting in the complete elimination of transonic tones. Also, at the downstream angle of 35°, the co-axial circular swirl jet radiates the lowest noise levels at all the frequencies, probably due to better centerline decay.

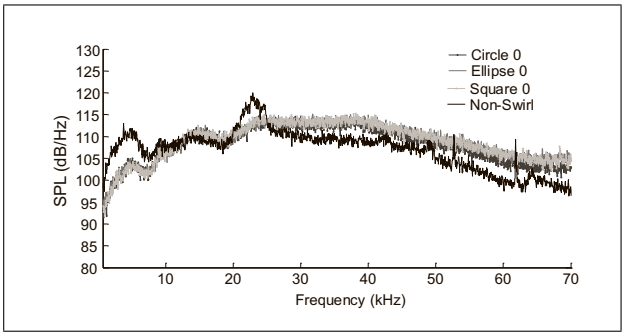

Figure 17. Far field sound pressure level spectra for NPR 2 and emission angle 90°.

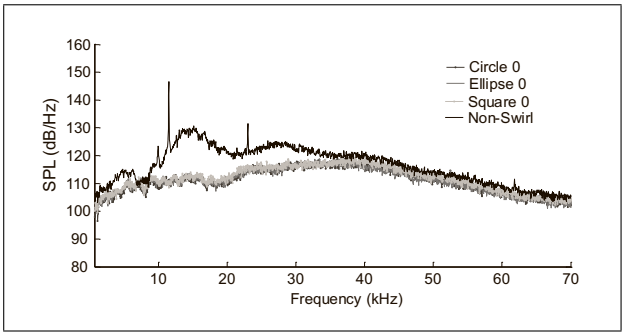

Figure 18. Far field sound pressure level spectra for NPR 4 and emission angle 130°.

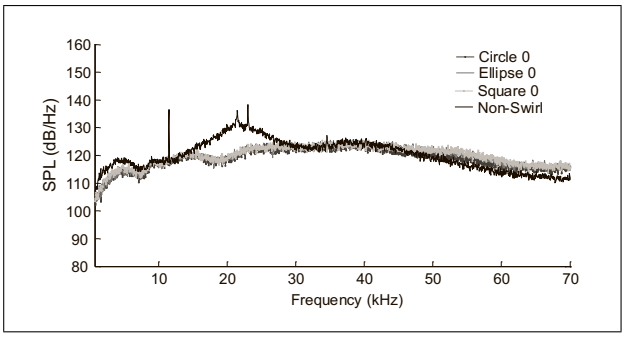

Figure 19. Far field sound pressure level spectra for NPR 4 and emission angle 90°.

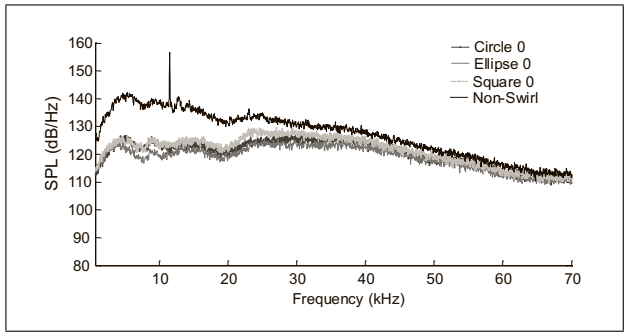

Figure 20. Far field sound pressure level spectra for NPR 4 and emission angle 35°.

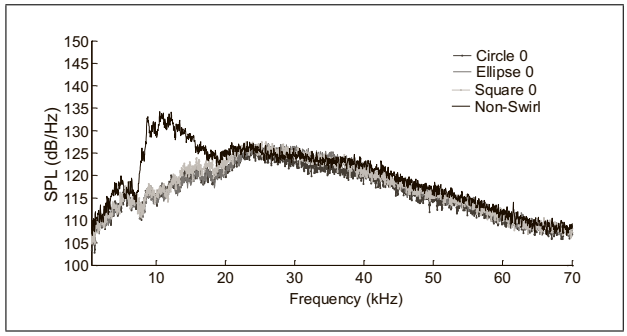

Figure 21. Far field sound pressure level spectra for NPR 6 and emission angle 130°.

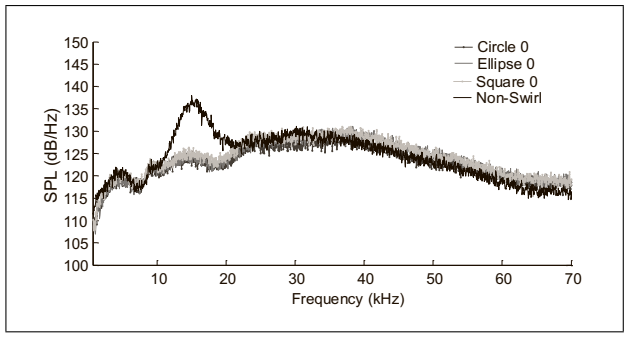

Figure 22. Far field sound pressure level spectra for NPR 6 and emission angle 90°.

At NPR 2, the spectra are almost similar to those for 0° vane angle jet cases as shown in Figure 17, for an emission angle of 90°. However, the high frequency noise components for the 30° vane angle jets are higher than those for the 0° vane angle jet cases. The increase in vane angle promotes the production of small scale turbulence structures which possess energy in the higher frequencies.

Figures 18 and 19 show the noise spectra of various co-axial jets for NPR 4 at emission angles of 130° and 90°, respectively. It is observed that the high frequency noise components are the highest for the 30° vane angle jet compared to the 0° vane angle jet (Figures 9 and 10). This indicates that the higher vane angle generates higher high frequency noise components compared to the lower vane angle. Similar to 0° vane angle jets, in this case also, screech tones and BSAN are eliminated. Figure 20 shows spectra at an emission angle of 35° for NPR 4. It is observed that the low frequency noise is lowest for the 30° vane angle jet compared to the 0° vane angle jet. Probably, this due to the large scale turbulence structures breaking down into smaller ones and thereby transferring the energies to the higher frequencies.

Noise spectra of various jets at NPR 6, at emission angles of 130° and 90° are shown in Figures. 21 and 22, respectively, for the 30° vane angle case. It is observed that there are no screech tones for all the cases shown. Also, the shock associated noise is mitigated by the 30° vane angle jets, in contrast with the observations for 0° vane angle jets. This shows the effects of vane angle and it is evident that increase in the vane angle leads to elimination of the BSAN for the co-axial circular and co-axial non-circular jets. However, the high frequency noise com-

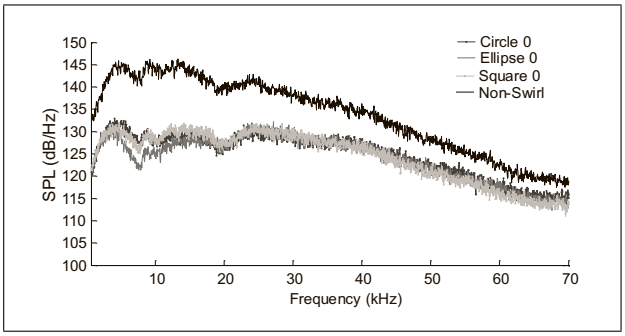

Figure 23. Far field sound pressure level spectra for NPR 6 and emission 8angle 35°.

ponents show an increase compared to 0° vane angle jets. Figure 23 shows the spectra at an emission angle of 35° at NPR 6. It is observed that the high frequency noise is lower for the 30° vane angle jet compared to 0° vane angle jets and non-swirl jet. This is probably due to the rapid centerline decay and enhanced mixing brought about by the increase in vane angle, leading to reduction in the noise levels in the downstream angles.

4. Directivity characteristics

This section deals with the directivity of overall sound pressure level (OASPL) for different vane angles, based on which the effects of vane angle are discussed.

4.1. Directivity of OASPL for 0° vane angle

Figure 24 compares the OASPL directivity for the non-swirl and co-axial circular and non-circular jets. The non-swirl jet emits the highest noise levels at all the emission angles due to the presence of multiple transonic tones. However, all the co-axial jets with 0° vane angle radiates the lowest noise compared to the non-swirl jet. The vortices shed from the trailing edge of the flat vanes enhance the mixing between the jet and ambient fluid and leads to a reduction of noise, and amplitude of transonic tone, compared to the non-swirl jet. Among the co-axial jets with 0° vane angle, the co-axial circular jet radiates the maximum OASPL compared to the co-axial ellipse and co-axial square jets. This is because; the transonic tone amplitudes are higher for the co-axial circular jet compared to co-axial ellipse and co-axial square jets. In addition, the high frequency noise components are also higher for the co-axial circular jets. These two points are the reason for the maximum noise levels emitted by the co-axial circular jet. The noise reduction achieved by the co-axial ellipse and co-axial square jets is around 10 dB, except at mid range emission angles.

The non-swirl jet OASPLs are lower for NPR 2 compared to the NPR 1.8 case (Figure 25), due to the disappearance of the transonic tones. All the co-axial jets with 0° vane angle radiate almost the same amount of noise. In the emission angle range of 70° < EA < 95°, the co-axial jets with 0° vane angle are noisier than the non-swirl jet.

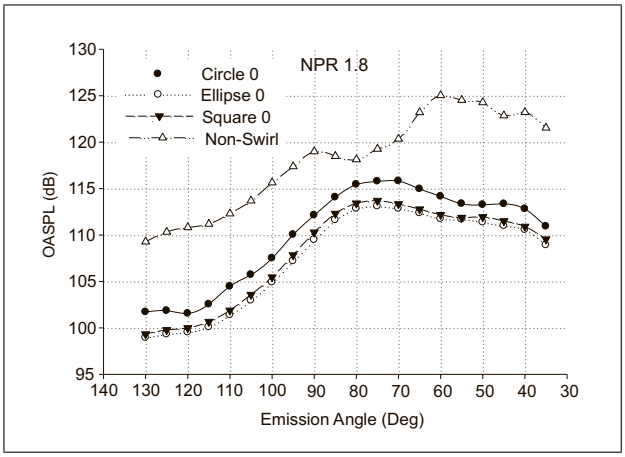

Figure 24. Directivity of OASPL for different microphone polar angle NPR 1.8.

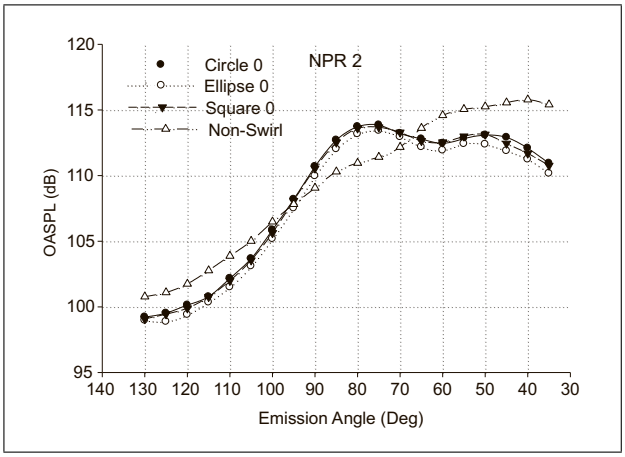

Figure 25. Directivity of OASPL for different microphone polar angle NPR 2.

At these emission angles the high frequency noise component is higher for the 0° vane angle jets, which causes an increase in the OASPL level. However, at downstream angles the noise levels are lower for the 0° vane angle jets compared to the non-swirl jet. The enhanced mixing and entrainment rates cause a reduction in the axial momentum, leading to lower noise levels in the downstream angles.

At NPR 4, the OASPLs of the co-axial circular and co-axial non-circular 0° vane angle jets are the lowest compared to the non-swirl jet, as shown in Figure 26. Especially, better noise reduction of around 12-15 dB is achieved at upstream angles. This is due to the elimination of the BSAN and screech tones by the 0° vane angle co-axial circular and co-axial non-circular jets.

Figure 27 shows the directivity of OASPL at NPR 6, and reveals that the non-swirl jet emits the maximum noise levels due to strong shock cells and their interactions with the downstream convecting turbulent structures. The co-axial circular jet radiates the least noise compared to the other jets. The co-axial square jet radiates maximum noise compared to co-axial circular and co-axial ellipse jets. The

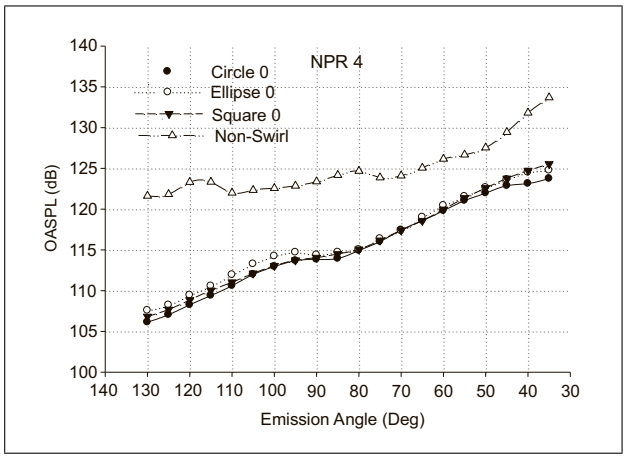

Figure 26. Directivity of OASPL for different microphone polar angle NPR 4.

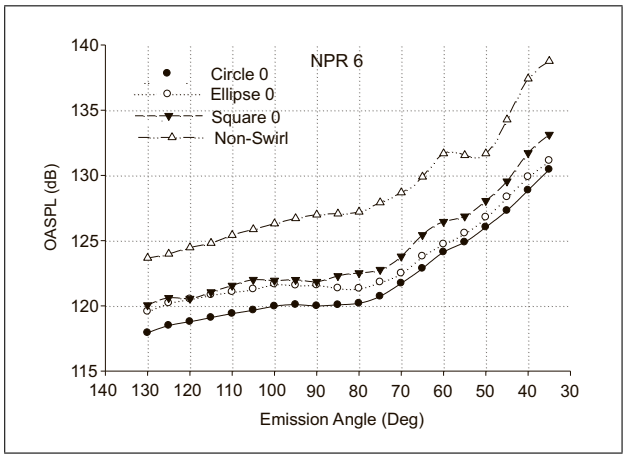

Figure 27. Directivity of OASPL for different microphone polar angle NPR 6.

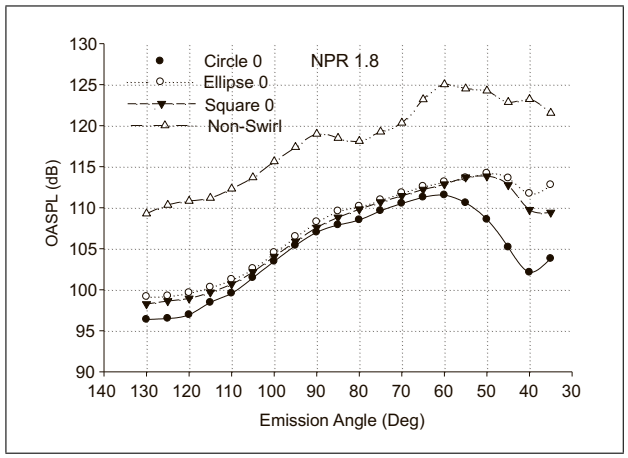

Figure 28. Directivity of OASPL for different microphone polar angle NPR 1.8.

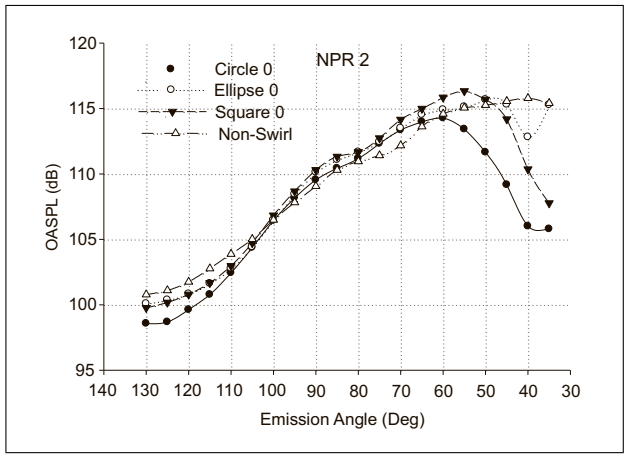

Figure 29. Directivity of OASPL for different microphone polar angle NPR 2.

shock associated noise is higher for the co-axial square jet (observed in the spectra for EA > 90°) compared to co-axial circular and co-axial ellipse jets. The co-axial circular jet with 0° vane angle efficiently eliminates the shock noise and lower the OASPL at NPR 6 compare to co-axial non-circular jets.

4.2. Directivity of OASPL for 30° vane angle

Figure 28 compares the OASPL for the flat vane angle of 30°. The co-axial circular jet radiates the lowest noise compared to other jets and around 13 dB noise reduction is achieved by the co-axial circular jet compared to the co-axial non-circular jet. Similarly, in the downstream angles, around 17 dB noise reduction is achieved by the co-axial circular jet, due to the reduction in axial momentum. However, the co-axial ellipse and co-axial square jets emit higher noise levels than the co-axial circular jet. This is due to the enhanced fine scale turbulent structures emerging from the co-axial ellipse and co-axial square jets. The corners of square jet induce four pairs of counter rotating streamwise vortices which enhance the mixing [14].

At NPR 2, the co-axial circular and co-axial non-circular swirl jets with 30° vane angle radiate the lowest noise levels in the upstream and downstream angles as shown in Figure 29. However, at midrange angles the co-axial circular and co-axial non-circular swirl jets emit higher noise than the non-swirl jet, due to the enhanced fine scale mixing. That is, the high frequency noise is highest for the co-axial swirl jets in the mid range emission angles.

The directivity of OASPL at NPR 6 is shown in Figure 30. The non-swirl jet emits the maximum noise due to the presence of strong shock cells. In this case also, the co-axial circular jet radiates the least amount of noise at all the emission angles compared to the other jets. All the co-axial swirl jets with 30° vane angle eliminate BSAN at NPR 6. The noise variations among the co-axial swirl jets are due to the enhanced mixing by the co-axial non-circular jets compared to the co-axial circular jet. The downstream noise reduction for all the co-axial swirl jet is due to the reduction of axial momentum by the co-axial swirl jets with higher entrainment rates.

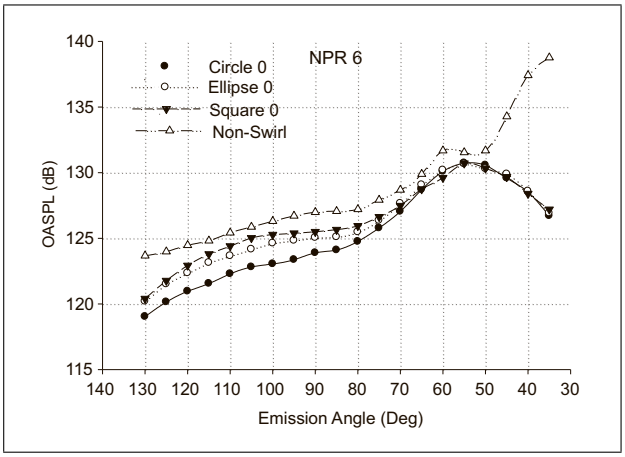

Figure 30. Directivity of OASPL for different microphone polar angle NPR 6.

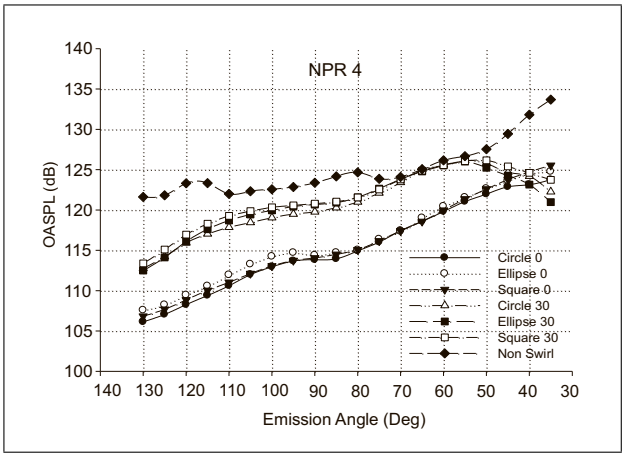

Figure 32. Directivity of OASPL comparisons between the vane angle of 0° and 30°, NPR 4.

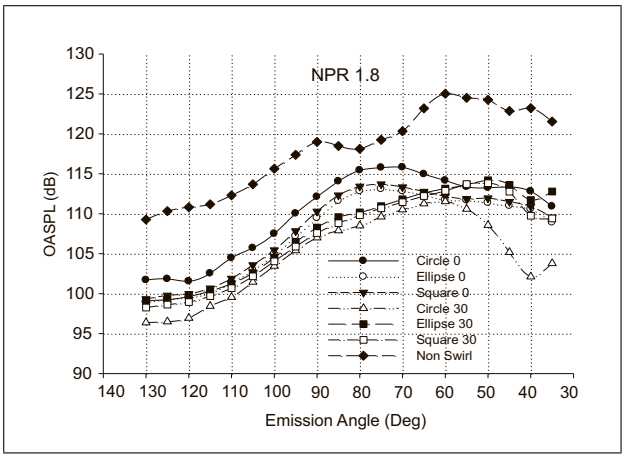

Figure 31. Directivity of OASPL comparisons between the vane angle of 0° and 30°, NPR 1.8.

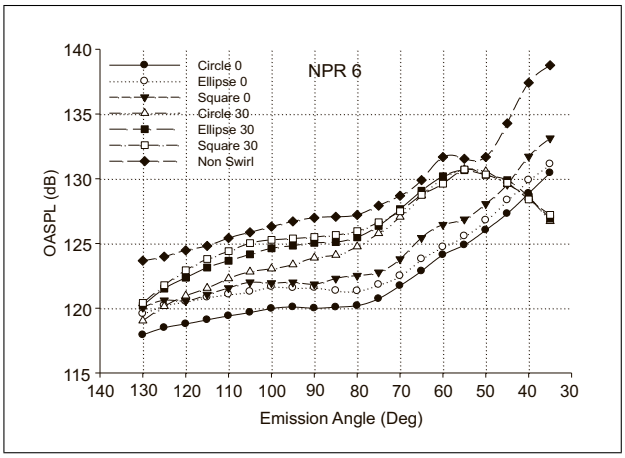

Figure 33. Directivity of OASPL comparisons between the vane angle of 0° and 30°, NPR 6.

4.3. Directivity of OASPL comparisons for 0° and 30° vane angle

The directivities of OASPL are compared for both the vane angles of 0° and 30° in Figure 31 for NPR 1.8. It is observed that the co-axial circular jet with the vane angle of 30° radiates the lowest noise at all the emission angles compared to the other jets. Co-axial circular jet with 0° vane angle radiates the highest noise among the other co-axial jets. Co-axial circular jet with 30° vane angle radiates the lowest noise compared to other jets, and around 14–16 dB noise reduction is achieved. At far downstream angles around 20 dB noise reduction is achieved. The complete elimination of transonic tones in the 30° vane angle swirl jets might be the reason for radiation of lowest noise levels compared to the 0° vane angle jets and non-swirl jet.

However, at NPR 4 and 6 the 0° vane angle jets radiate the lowest noise compared to the co-axial jets with 30° vane angle, as shown in Figure 32 and 33. Co-axial circular jet with vane angle of 0° radiates the lowest noise compared to all other jets and around 5–15 dB and 5–7 dB noise reduction is achieved compared to the non-swirl jet, for NPR 4 and 6, respectively. The reason for the 30° vane angle co-axial swirl jets to radiate the higher noise than the 0° vane angle co-axial jets is due to the enhanced fine scale mixing from the higher degree vane angles.

4.4. Directivity of OASPL comparisons for non-swirl jet with and without screech

Figures 34 and 35 show the spectra for the non-swirl jet with and without screech tones at NPR 4. The screech tone is deleted artificially in the noise spectra in order to compare the screech free OASPLs of the various jets. It may be noted that only the non-swirl jets display screech, and therefore, the truncation of screech has been applied only on the non-swirl jet spectra. After the deletion of screech tones, the OASPL values obtained may not be the same as the corresponding screech-free cases. The procedure is carried out for comparison purposes only.

Figure 36 compares the OASPL at NPR 4, for the all the jets, including non-swirl jet with screech tone removed. At most upstream angles and downstream angles the non-swirl jet radiates highest noise compared to the 0° and 30° vane angle jets. However, the emission angles between 115° > EA > 45°, all the 30° vane angle swirl jets ra-

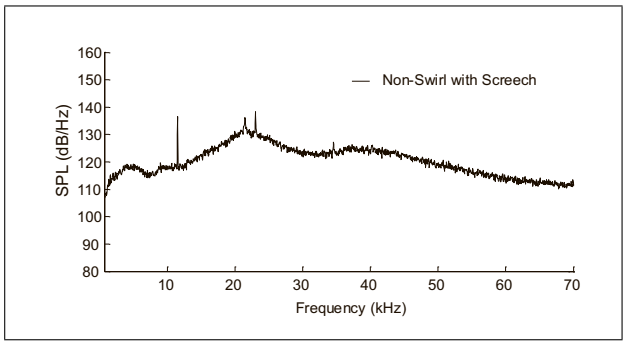

Figure 34. Spectrum for NPR 4 and emission angle 90° with screech tone.

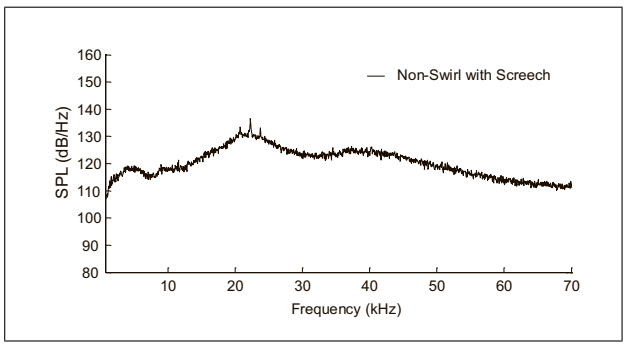

Figure 35. Spectrum for NPR 4 and emission angle 90° without screech tone.

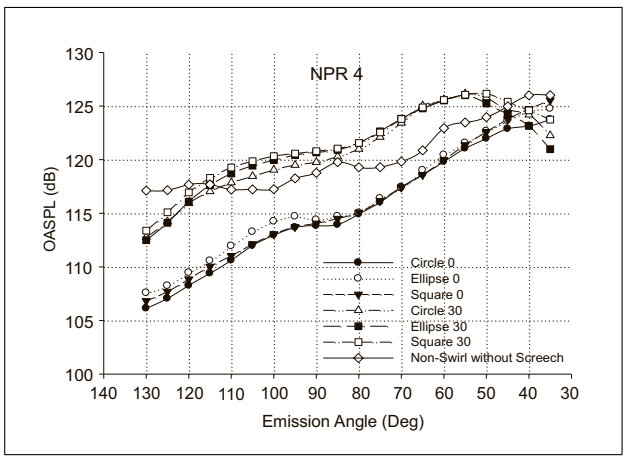

Figure 36. Directivity of OASPL comparisons with non-swirl jet without screech tone, NPR 4.

diate highest noise due to the enhancement of the high frequency noise, which is observed in the corresponding spectra. Moreover, all the 0° vane angle jets radiate the lowest noise levels compared to the screech free non-swirl and 30° vane angle swirl jets at all the emission angles.

5. Flow field characteristics

The pitot survey reveals the total pressure (Pt) variation along the centerline of the jets. The measurements are qualitative due to the shock dominated field. However, the measurements are useful for comparing the number of shock cells and shock strength in different jets. Also,

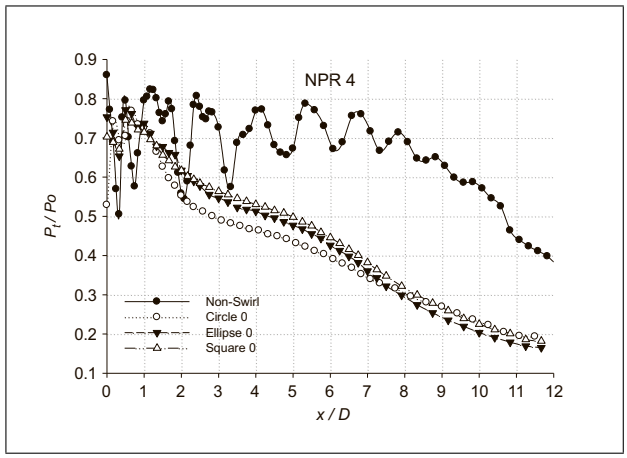

Figure 37. Centerline pitot pressure variation at NPR 4.

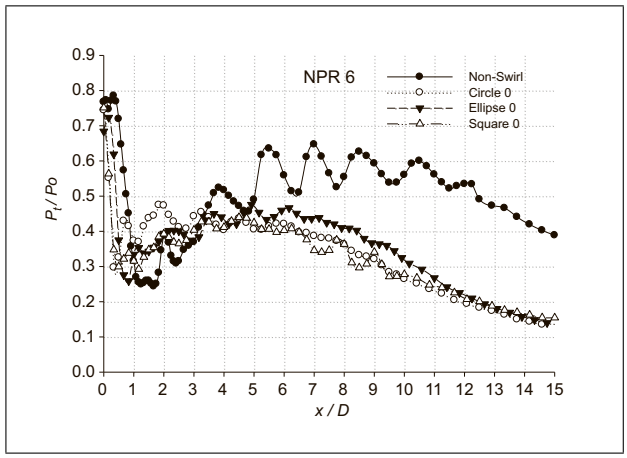

Figure 38. Centerline pitot pressure variation at NPR 6.

measuring the centerline decay is an indirect measure of mixing of the jet fluid with the ambient.

5.1. Centerline pitot pressure decay for 0° vane angle

Figure 37 shows the centerline decay of non-swirl jet and various co-axial swirl jets at NPR 4. The non-swirl jet shows oscillations in the profile due to the shock cells and the core extends to around $x/D = 11$. The strength of shocks in non-swirl jet is reduced due to the mixing taking place between the jet fluid with the ambient. However, for the 0° vane angle jet, the shock cells are weak, and the core extends to around $x/D = 1$ only. Around 90% reduction in core length is achieved by the co-axial swirl jets compared to the non-swirl jet. The 0° annular vanes generate vortices from the blades that travel over the primary jets along the jet center axis and weaken the shock cells and enhance the mixing. Hence, the co-axial jet with 0° vane angle is much effective in controlling the shocks compared to the non-swirl jet. The co-axial circular jet decays more rapidly compared to co-axial non-circular jets.

A strong pressure deficit is observed for all the jets at a highly under expanded condition of NPR 6, as shown in Figure 38. The flow visualization study confirms the

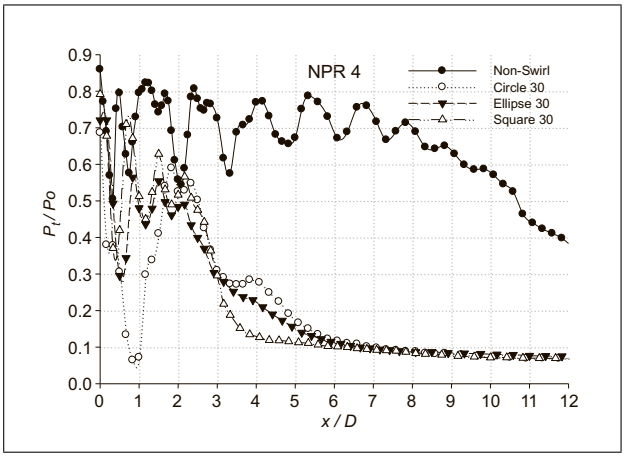

Figure 39. Centerline pitot pressure variation at NPR 4.

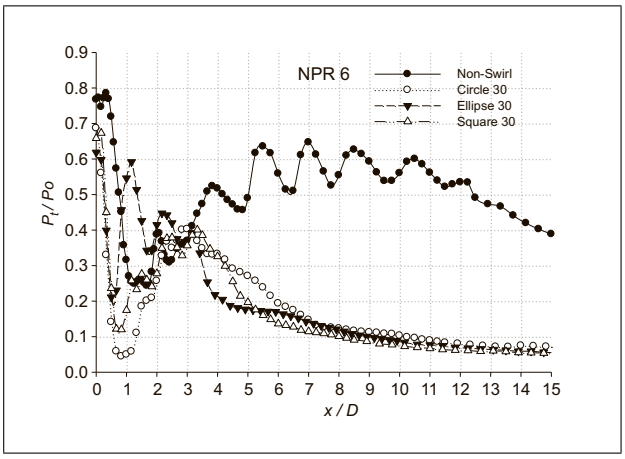

Figure 40. Centerline pitot pressure variation at NPR 6.

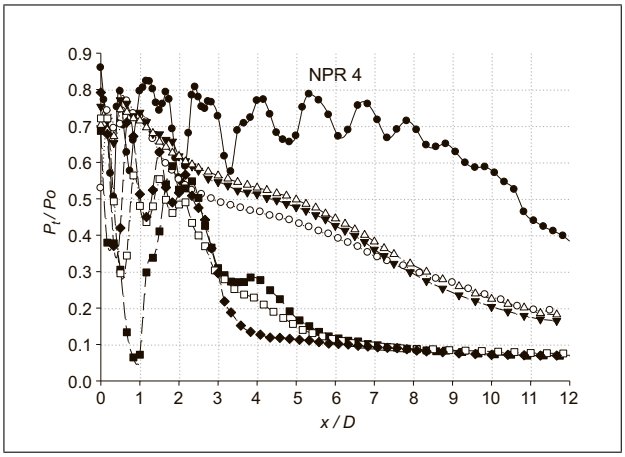

Figure 41. Comparison of centerline pitot pressure decay for 0° and 30° vane angle, NPR 4.

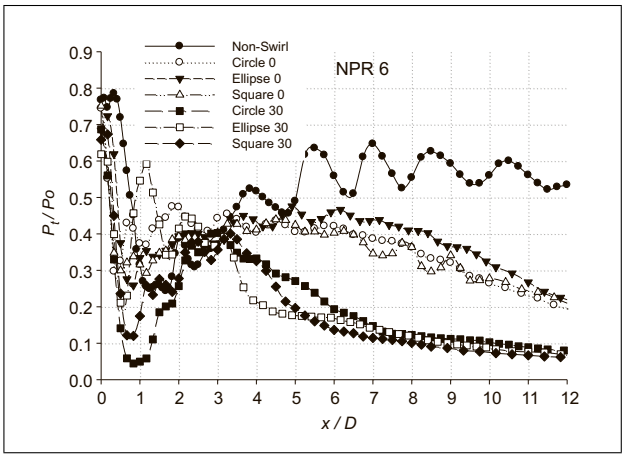

Figure 42. Comparison of centerline pitot pressure decay for 0° and 30° vane angle, NPR 6.

presence of Mach disk at this NPR. The shock-cell region in the non-swirl jet extends to around $x/D = 13$, which is higher than the value at NPR 4. The co-axial ellipse and square jets with 0° vane angle show several mild shock cells and their core lengths extend to around $x/D = 10$. The co-axial circular jet shows a short core length of around $x/D = 6$. The interaction of the annular vortices flow with the circular shape hub flow is more effective in the destruction of the shock cells compared to ellipse and square hubs.

5.2. Centerline pitot pressure decay for 30° vane angle

Figure 39 shows that at NPR 4, more than 75% reduction ($2.5D$) in the core length is seen for the co-axial swirl jets with 30° vane angle compared to the non-swirl jet. Further, it is observed that after the end of the core region the centerline pressure decays more rapidly compared to the 0° vane angle cases. This shows the effect of vane angle in inducing decays of the centerline velocity by way of enhanced mixing.

The co-axial swirl jets with 30° vane angle show core lengths of around $x/D = 3.5D$ at NPR 6, as shown in Figure 40. At NPR 6, the shock strengths and spacings are much lower for 30° vane angle jets compared to 0° vane angle jets. The increase in vane angle causes the weakening of shock cells and enhanced mixing. The annular swirl promotes the mixing and exchange of momentum in the radial direction in contrast to the non-swirl jets, which helps faster equilibration of pressure of the jet fluid with the ambient. The presence of swirl also helps to weaken the shocks.

5.3. Comparison of centerline pitot pressure decay for 0° and 30° vane angle

Comparison of centerline total pressure measurements between the 0° and 30° vane angles are discussed in this section.

It is observed that the centerline pressure decays more rapidly for all the 30° vane angle jets compared to the 0° vane angle case as shown in Figure 41 at NPR 4 (For labels refer to Figure 42). This shows the effect of vane angle in inducing decay of the centerline velocity, which is an indirect measure of enhanced mixing. Also, the 30° vane angle co-axial circular swirl jet decays more rapidly compared to other jets. Similar behavior is observed for the NPR 6 also,

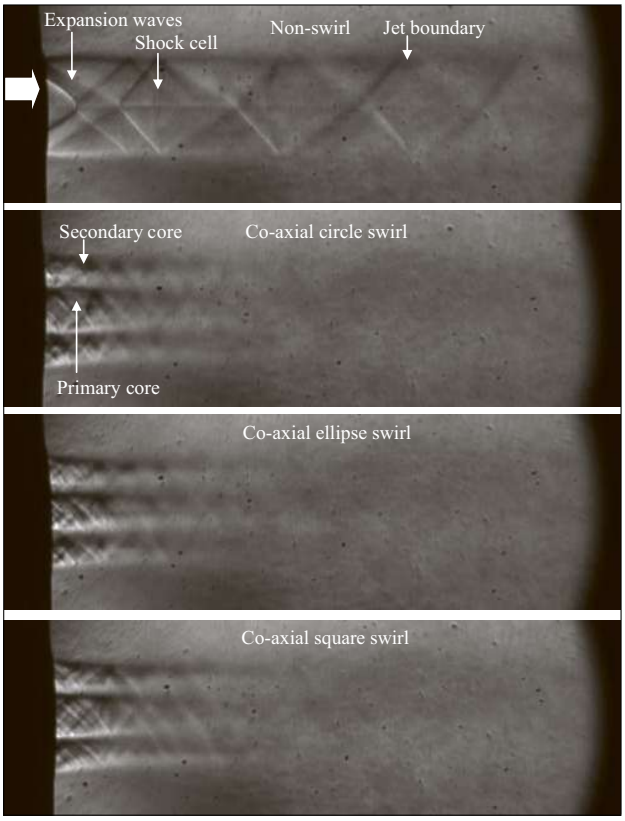

Figure 43. Schlieren photographs for NPR 4 and 0° flat vane angle.

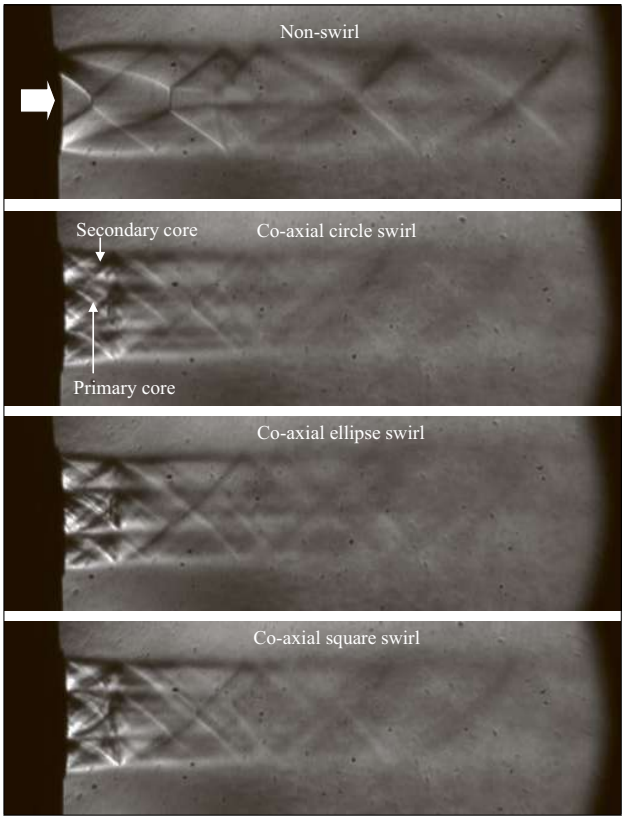

Figure 44. Schlieren photographs for NPR 6 and 0° flat vane angle.

as shown in Figure 42. Further, it is observed that the shock cell elimination by the 30° vane angle swirl jets is higher compared to the 0° vane angle jets and the non-swirl jet. Weak shock cells are observed for all the 0° vane angle jets, up to around $x/D = 10D$, while for the 30° vane angle swirl jet, it is less than $5D$. However, the OASPL levels are higher for the 30° vane angle swirl jets, compared to 0° vane angle jets, even though the shock cell lengths are lower. This shows that the mixing enhancement by the 30° vane angle swirl jet is the highest, which enhances the turbulent mixing noise (especially the high frequency noise, which is observed in the spectra). Hence, the OASPL levels are higher.

6. Flow visualization

The flow visualization study is carried out in order to understand the shock-cell structures of the various jets. The shock associated noise contribution to the OASPL is dominant and it is necessary to understand the shock-cell structures and shock strengths at different NPRs. Flow visualization studies at NPR 4 and 6 are discussed for the vane angles of 0° and 30° .

6.1. Schlieren photographs for 0° flat vane angle

Figure 43 shows schlieren photographs for 0° flat vane angle at NPR 4. The non-swirl jet shows a series of shock cells in the jet core. The shock strengths and the number of shock cells are higher for the non-swirl jet compared to the co-axial jets with 0° vane angle. The co-axial jets with 0° vane angle jets clearly show the presence of separate primary and secondary core shock cells. Further, it is clearly visible that the shock cells are very weak.

Figure 44 shows the schlieren photographs for NPR 6. A strong Mach disk is observed for the non-swirl jet, followed by a series of strong shock cells. The expansion waves and the reflecting waves are clearly visible. The non-swirl jet is a disk nozzle with disk width of 6 mm. Therefore, a double shock like structure manifests in disk nozzles, possibly due to two sets of expansion fans, one from the leading edge of the disk nozzle and another from the trailing edge of the disk nozzle.The co-axial jets with 0° vane angle jets show a reduction in shock cells and the number of shock cells, compared to the non-swirl jet.

The vortices from the vanes promote mixing, and their interactions with the primary core causes a reduction of shock strength and number of shock cells. The shocks are stronger at NPR 6 compared to NPR 4, especially in the near field. The primary and secondary cores of the co- axial circular jet interact well compared to the co-axial non-circular cases. From these observations, it is clear that the co-axial jets with 0° vane angle efficiently mitigates the shock-cells compared to a non-swirl jet. The shock destruction is the main reason for the lower noise levels observed in the co-axial jets compared to the non-swirl jets.

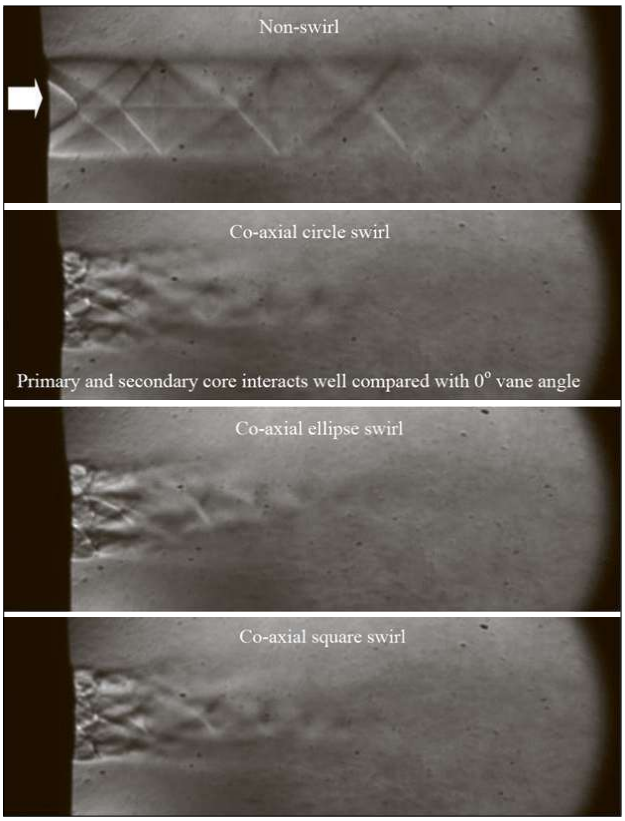

Figure 45. Schlieren photographs for NPR 4, 30° flat vane angle.

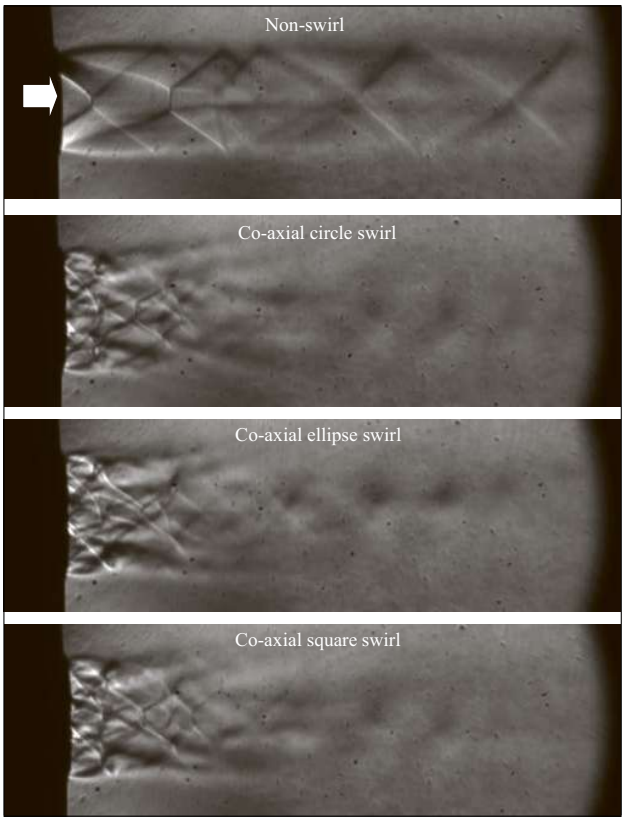

Figure 46. Schlieren photographs for NPR 6 and 30° flat vane angle.

6.2. Schlieren photographs for 30° flat vane angle

Schlieren photographs for 0° and 30° flat vane angle at NPR 4 and 6 are shown in Figures 45 and 46. At 30° vane angles the primary and secondary cores interact more aggressively compared to 0° flat vane angle. This shows that, the effects of the vane angles. Keeping NPR constant and increasing the vane angle makes the shock structures very complex and the interaction between the primary and secondary core more. The core lengths reduce to a great extent for the co-axial swirl jets compared to non-swirl jet at NPR 6. The spread of the co-axial circular jet seems to be higher than the co-axial ellipse and co-axial square jets. The near field of co-axial swirl jets shows a very complex structure of shock-cells and their interactions.

When we compare the pitot measurements with the schlieren images, the shock cell lengths in the schlieren images may look longer. This is because the schlieren images are merely qualitative whereas the centerline pitot measurements are quantitative with respect to x/D.

7. Use of co-axial vane jets in aircraft engines

It is observed from the far field acoustic studies that the co-axial vane jets with vane angles of 0° and 30° radiate lower noise levels compared to the non-swirl jet for the same nozzle pressure ratio. Also, the supersonic noise components such as screech tones and shock associated noise are also well mitigated by the co-axial vane jets. The flow field study shows a reduction in the number of shock cells, shock cell spacing and shock strength, compared to the non-swirl jets. These phenomena leads to mitigation of noise radiation from co-axial vane jets compared to non-swirl jets.

Aircraft engines emit higher amounts of noise, especially during take-off and such noise is uncomfortable to those who work/stay near the airport. Also, the screech and BSAN components may deteriorate the aircraft structures. The use of co-axial vane jets is highly beneficial in terms of noise reduction in aircraft engines applications, and the screech tones, BSAN can be completely eliminated. However, this benefit would be accompanied by a penalty in the form of loss in thrust of the engines. The passive control devices (vanes) may also add to the weight of the aircraft. Thus, a careful consideration must be made for incorporating this strategy in aircraft engines. For instance, zero degree vane angle jets may turn out to be very good candidates for achieving higher noise reductions with lower pressure losses and thrust penalty. Furthermore, apart from aircraft industries, the results obtained from this study may be useful for enhancement of mixing and reduction of noise in other engineering industries such as industrial mixing systems, manufacturing, and so on.

8. Conclusions

In this work, experimental acoustic far field and flow field studies on co-axial circular and co-axial non-swirl jets

with the vane angles of 0° and 30° are conducted. The co-axial circular and non-circular jets are efficient in noise reduction at all the NPRs tested compared to the non-swirl jets. Co-axial jets with the vane angles of 0° and 30° jets reduced the OASPL levels around 10-13 dB at NPR 1.8 compared to the non-swirl jet. Increase in flat vane angles enhances the spread rates and decreases the axial momentum. Transonic tones, screech tones and shock associated noise are almost eliminated by the co-axial jets, irrespective of the vane angle. At NPR 6, co-axial circular jet with 0° vane angle reduced the OASPL levels by around 6 dB compared to the non-swirl. For the flat vane angle of 0° at low NPRs, the co-axial non-circular jets are efficient in noise suppression compared to the co-axial circular and non-swirl jets, while at NPR 6 the co-axial circular jet is efficient. However, for the flat vane angle of 30° the co-axial circular jet is efficient in noise suppression at all the NPRs. The core reduction is high as much as 90% in the case of co-axial jets compared to the non-swirl jets. Similarly, the co-axial jets are efficient in shock destruction and reduction in the number of the shock cells. The core reduction and shock destruction increase with increase in vane angles.

References

[1] E. Gutmark, K. C. Schadow, K. J. Wilson: Noncircular jet dynamics in supersonic combustion. Journal of Propulsion and Power **5** (1989) 529–533.

[2] X. Min-Yi, T. Xing-Qing, Y. Dan-Ting, Z. Jian-Peng, M. Jian-Chun, G. J. Nathan, P. A. Kalt: Effect of non circular orifice plates on the near flow field of turbulent free jets. Chinese Physics B **23** (2014) 124703 (1–9).

[3] A. Hashiehbaf, G. P. Romano: Particle image velocimetry investigation on mixing enhancement of non-circular sharp edge nozzles. International Journal of Heat and Fluid Flow **44** (2013) 208–221.

[4] A. K. Gupta, D. G. Lilley, N. Syred: Swirl flows. Abacus Press, 1984.

[5] Y. Fu: Aerodynamics and combustion of axial swirlers. Ph.D. Thesis, Department of Aerospace Engineering and Engineering Mechanics, University of Cincinnati, 2009.

[6] E. Kilik: The influence of swirler design parameters on the aerodynamics of the downstream. Ph.D. Thesis, School of Mechanical Engineering, Cranfield Institute of Technology, UK, May 1976.

[7] T. J. S. Jothi, K. Srinivasan: Transonic resonance tones in orifice and pipe jets. International Journal of Aeroacoustics **12** (2013) 103–122.

[8] C. K. W. Tam: Supersonic jet noise. Annual Review of Fluid Mechanics (1995) 17–43.

[9] H. Y. Lu, J. W. Ramsay, D. L. Millier: Noise of swirling exhaust jets. AIAA Journal **15** (1997).

[10] Y. K. Yu, R. H. Chen: A study of screech tone noise of supersonic swirling jets. Journal of Sound and Vibration (1997) 698–705.

[11] M. Samimy, K. B. M. Q. Zaman, M. F. Reeder: Effect of tabs on the flow and noise field of an axisymmetric jet. AIAA Journal **31** (1993) 609–619.

[12] D. Papamoschou, M. Debiasi: Noise measurements in supersonic jets treated with the Mach wave elimination method. AIAA journal **37** (1999) 154–160.

[13] A. Kiran: Jet noise: aeroacoustic distribution of a subsonic co-axial jet. Ph.D. Dissertation, University of Warwick, 2008.

[14] W. R. Quinn: Streamwise evolution of a square jet cross section. AIAA journal **30** (1992) 2852–2857.